PHYSICAL REVIEW C

NUCLEAR PHYSICS

Proton scattering from ^{12}C between 120 and 200 MeV and the optical potential

H. O. Meyer, P. Schwandt, W. W. Jacobs, and J. R. Hall

Indiana University Cyclotron Facility, Bloomington, Indiana 47405

(Received 22 September 1982)

Cross sections and analyzing powers are presented for ^{12}C$(\vec{p},p)^{12}$C elastic scattering at 122 and 160 MeV. The data cover a large angular range (up to $\theta_{\text{lab}} = 154°$) and extend to lower energies an earlier, similar measurement at 200 MeV. The complete data set is analyzed in the framework of the optical model. Besides the standard Woods-Saxon potential, nonstandard radial shapes for the central and the spin-orbit potentials are investigated. Although the number of free parameters for the nonstandard potential is substantially reduced from the standard potential, it provides an improved fit to the data and a description of ^{12}C$(p,p)^{12}$C scattering with a simple monotonic energy dependence in the region 100–200 MeV. The characteristic features of the nonstandard potential are reproduced by microscopic theories.

NUCLEAR REACTIONS ^{12}C$(\vec{p},p)$, $E_p = 122$, 160 MeV, $\theta_{\text{lab}} = 6°-154°$; measured $\sigma(\theta)$ and $A(\theta)$; optical-model analysis, including data at 200 MeV, nonstandard potential shapes, energy dependence of optical potential.

I. INTRODUCTION

As early as 1966, Elton[1] suggested that the optical potential for proton-nucleus scattering at medium energies differs in shape from the customarily used Woods-Saxon (WS) form. A clear experimental verification of this proposal was seen recently[2,3] in ^{12}C$(p,p)^{12}$C elastic scattering at 200 MeV. It also has been established that the sensitivity to deviations from standard potential shapes is enhanced by inclusion of scattering data at high momentum transfer.[3] The main departure from the standard WS shape occurs in the real central potential which, in the nuclear interior, is found to be less attractive than near the surface. This phenomenological finding is in fact expected theoretically, following either of two quite different approaches. In the first, the proton nucleus interaction is evaluated in a nonrelativistic framework[4] starting from an effective nucleon-nucleon (NN) interaction.[5] Here, the shape modification of the potential in the interior region arises from the antisymmetrization of the projectile-target system. In the second approach, the nucleon-nucleus scattering is described by the rela-

tivistic Dirac equation. The Dirac potential can be constructed from a simple NN force as would arise from the exchange of effective scalar and vector mesons, but is often parametrized phenomenologically in terms of WS forms. Here, the shape modification arises in the transformation of the Dirac potential to a phase-equivalent Schrödinger potential.

The result that a nonstandard optical potential is required to explain proton elastic scattering from ^{12}C at 200 MeV calls for an extension of such measurements to other energies in order to derive a phenomenological energy dependence of such a potential which then in turn can be compared with theoretical expectations. In this paper, we present cross section and analyzing power measurements for ^{12}C$(p,p)^{12}$C elastic scattering over the full angular range up to $\theta_{\text{c.m.}} = 156°$ at the additional energies of 122 and 160 MeV. The experimental procedure and the data are discussed in Sec. II A. Computational techniques are explained in Sec. II B. The various potential options for the optical model analysis considered in this work are introduced in Sec. III, while the analysis of the available data at all three energies (122, 160, and 200 MeV) is presented in Sec. IV. Conclusions and final remarks are given in Sec. V.

II. TECHNIQUES

A. Measurements

The measurements reported here were carried out using the polarized proton beam from the Indiana University Cyclotron Facility (IUCF). The beam intensity on target was varied from a few to about 100 nA depending on scattering angle (and target thickness) in order to achieve reasonable counting rates and electronic deadtimes. The beam polarization (typically 70%) was measured using a technique described in Ref. 6. Several self-supporting targets were used, ranging in thickness from 2 to 132 mg/cm^2. The thickest target was enriched in ^{12}C. The same targets were used in this experiment as in the earlier measurement[2,3] at 200 MeV, providing a consistent absolute normalization for all three data sets mentioned in this paper. The actual bombarding energies for the present investigation were $T = 121.9$ and 159.6 MeV.

The experimental setup, i.e., the magnetic spectrometer and the associated focal plane detector arrangement, and details about angular acceptance, beam charge integration, and the measurement of electronic deadtime during the data acquisition, were completely analogous to the 200 MeV experi-

ment and are described in detail in Ref. 2.

Corrections for deadtime losses (5—10%) and for the finite angular acceptance of the spectrometer (1—2%) were applied to the data. Where necessary, background arising from accidental coincidences between the focal plane detector elements was determined from the spectrum below and above the elastic peak and subtracted. The experimental uncertainties of the data contain the statistical error (including the statistical error of the background subtraction, where applicable), an error resulting from an uncertainty in setting the scattering angle ($\pm 0.05°$), and an estimated error for incomplete charge collection at scattering angles $\theta_{lab} < 24°$ where a small Faraday cup inside the scattering chamber was used. Not included is the absolute normalization uncertainty of the cross section dominated by imprecise knowledge of the target thickness, which is estimated to be 5—10%.

The results of the present experiment are displayed as solid circles in Fig. 1. Cross sections are given relative to the Rutherford cross section as defined in Eq. (4) below. Numerical values of the experimental results are available on request from IUCF. Also displayed in Fig. 1 are measurements obtained previously at 200 MeV (open circles, Refs.
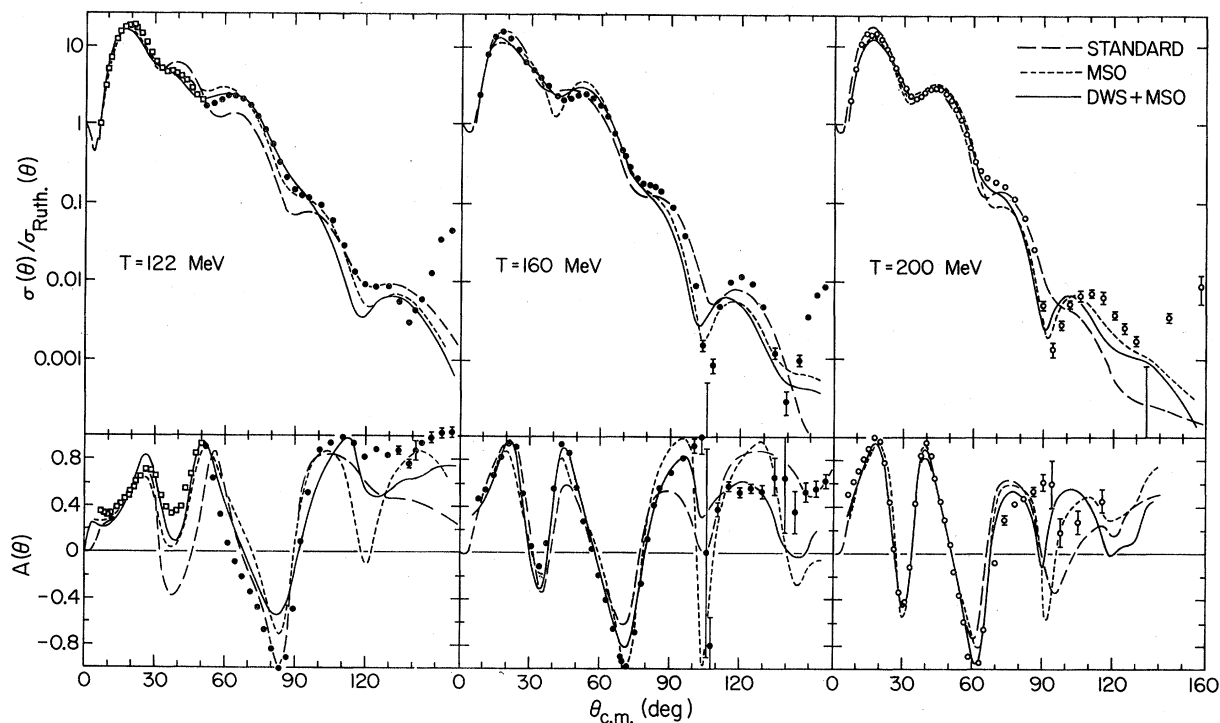

FIG. 1. Cross section and analyzing power angular distributions for $^{12}C(p,p)^{12}C$ elastic scattering at 122, 160, and 200 MeV. The solid circles represent the present measurements, the open squares are from Ref. 7, and the open circles are from Refs. 2 and 3. The three curves using different parametrizations of the optical potential are discussed in the text.

2 and 3) and at forward angles at 122 MeV (open squares, Ref. 7).

B. Computations

The optical model calculations presented here were carried out using the code SNOOPY8.[8] In addition to using the relativistic center-of-mass wave number

$$\left\{ \frac{d^2}{d\rho^2} + \left[1 - \frac{2(\sqrt{s} - M)[U_C(\rho) + U(\rho)]}{(\sqrt{s} - M)^2 - m^2} - \frac{l(l+1)}{\rho^2} \right] \right\} F_{lj}(\rho) = 0 .$$

(3)

In the above equations m, M, z, and Z are the masses and charges of the projectile and target, respectively, T is the laboratory kinetic energy, $s = (m + M)^2 + 2MT$, $\rho = kr$, α is the fine structure constant, β the projectile laboratory velocity, and U_C is the Coulomb potential. The corresponding Rutherford cross section has the form

$$\sigma_{\text{Ruth}}(\theta) = (\eta / 2k)^2 \sin^{-4}(\theta / 2) .$$

(4)

In calculations with the optical model at medium energies, care has to be taken regarding the appropriate choice of the step size in the integration of the differential equation. Too large a step size leads to unreliable results for the very small cross sections at high momentum transfer. This error is caused by the truncation of the Taylor series used to describe the solution locally; it thus depends on the method of integration used and becomes more critical for shorter wavelengths, i.e., increasing energy. For the present calculations a maximum step size of smaller than 0.05 fm was found necessary. The matching of the wave function of the scattered proton to the external, nonrelativistic Coulomb wave functions (but with relativistic values for the arguments η and ρ) was done at $r = 10.5$ fm.

III. OPTIONS FOR POTENTIAL PARAMETRIZATIONS

A. Standard parametrization

The nuclear optical potential $U(r)$ in Eq. (3) consists of complex central and spin-orbit terms. Customarily, the following parametrization is used to describe $U(r)$:

$$U(r) = V_R f_R(r) + iW f_W(r)$$
$$+ \lambdabar_\pi^2 [V_{\text{so}} g_{R\text{so}}(r) + iW_{\text{so}} g_{W\text{so}}(r)] \vec{\sigma} \cdot \vec{L} ,$$

(5)

where

$$f_i(r) = [1 + \exp\{(r - r_i A^{1/3})/a_i\}]^{-1}$$

(6)

$$k = (M / \sqrt{s})[T(T + 2m)]^{1/2}$$

(1)

and Coulomb parameter

$$\eta = zZ\alpha / \beta ,$$

(2)

the potential in the radial Schrödinger equation was scaled by an energy-dependent factor to account for relativistic effects,[8,9] resulting in

and

$$g_j(r) = (1/r)(d/dr)[1 + \exp\{(r - r_j A^{1/3})/a_j\}]^{-1} .$$

(7)

In this parametrization, all four potentials which contribute to $U(r)$ are of Woods-Saxon (WS) form or derivatives of WS forms. Almost all proton optical model calculations to date have been carried out with this prescription for the radial dependence of $U(r)$; the calculations in this paper using this parametrization will be labeled STANDARD.

Recently, as mentioned in the Introduction, evidence has been mounting that the radial shape of at least parts of the standard potential has to be modified in order to improve the description of proton elastic scattering data at medium energies. The two possible modifications which we believe are most important are introduced in the next two subsections (III B and III C).

B. Modified real central potential

For medium energy proton scattering, the real part of the central potential is less attractive in the nuclear interior than near the surface. This was first suggested by Elton's analysis[1] of ^{56}Fe$(p,p)^{56}$Fe scattering at 185 MeV, but only recently has clear experimental evidence been found[2] for such a feature of the potential in ^{12}C$(p,p)^{12}$C scattering at 200 MeV. We note that microscopic derivations of the optical potential for finite nuclei,[4] or based on realistic nuclear matter calculations[10] in a local density approximation, predict the same qualitative behavior for this potential. Phenomenologically, in order to allow for the appropriate flexibility in the description of the real central potential $V_R f_R(r)$ in the nuclear interior, we substitute in Eq. (5) the expression

$$V_R f_R(r) \equiv V_{R1} f_{R1}(r) - V_{R2}[f_{R2}(r)]^2 ,$$

(8)

where the form factors $f_{R1}(r)$ and $f_{R2}(r)$ are again given by Eq. (6). Note that the imaginary central

potential is unaffected by this change and is still of the standard WS form as is expected microscopically[4,10] in the energy region investigated here. The shape modification in Eq. (8) introduces three new parameters. Calculations using this double Woods-Saxon form we denote by DWS.

C. Semimicroscopic spin-orbit potential

If the effective NN spin-orbit interaction is of sufficiently short range (compared to nuclear dimensions), it has been shown[11] that any microscopically derived nucleon-nucleus spin-orbit potential is proportional to $(1/r)(d/dr)\rho(r)$, where $\rho(r)$ is the point nucleon density of the target nucleus. Since the long-range one-pion exchange component is missing in the NN spin-orbit force V_{LS}, it is reasonable to expect that V_{LS} is a sufficiently short-range interaction. On the basis of this argument, we introduce a new parametrization for the spin-orbit part of the potential $U(r)$ [Eq. (5)], where the form factors $g_{Rso}(r)$ and $g_{Wso}(r)$ are replaced by a common, parameterfree $g_{Mso}(r)$, while the complex strength will be treated phenomenologically,

$$g_{Rso}(r)=g_{Wso}(r)$$

$$\equiv g_{Mso}\equiv(1\ \text{fm}^3)\cdot(1/r)(d/dr)\rho(r)\ . \qquad (9)$$

Here, r is in fm and $\rho(r)$ in fm^{-3}, such that

$$\lambda_\pi^{\,2}g(r)=(2\ \text{fm}^2)g(r)$$

is dimensionless. The nuclear point density $\rho(r)$ for ^{12}C that we used in the present calculations has been obtained in the framework of the single-particle shell model constrained to match the experimental charge density[12] and neutron and proton removal energies. The resulting $\rho(r)$ was found to be well approximated by a sum of two WS forms as follows:

$$\rho(r)=0.195[1+\exp(2.04r-4.32)]^{-1}$$

$$-0.037[1+\exp(3.57r-2.29)]^{-1}\ , \qquad (10)$$

where r is in fm and $\rho(r)$ in fm^{-3}. The density as given by Eq. (10) is displayed as the solid line in Fig. 2. Also shown is a fully microscopic calculation[4,13] (short dashes) of the spin-orbit potential using the matter density $\rho(r)$ as given by Eq. (10) and an effective NN interaction[14] based on the Hamada-Johnston potential. This may be compared with the radial shape of $g_{Mso}(r)$ given by Eq. (9), arbitrarily normalized (dashed line in Fig. 2). It is obvious that the latter indeed is a very good approximation of the shape of the microscopically derived spin-orbit potential. Calculations using the representation given in Eq. (9) for form factors of the spin-orbit potential will be denoted by MSO. We point out that the
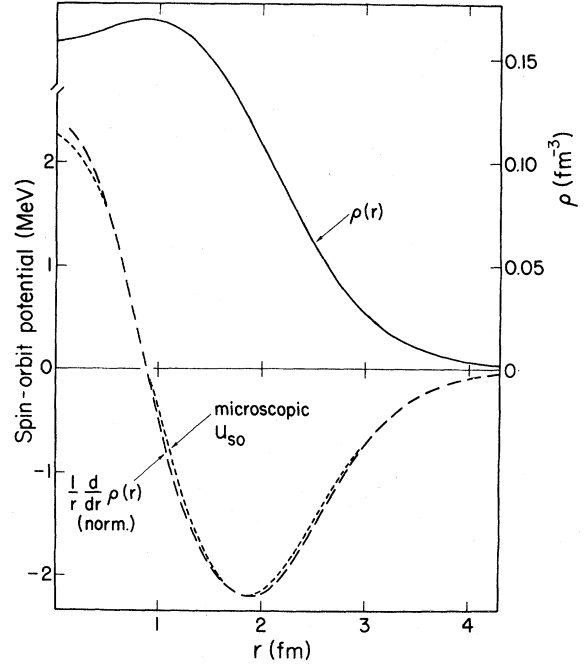

FIG. 2. Point-nucleon density of ^{12}C as described by Eq. (10) (solid curve), microscopically derived spin-orbit potential (short dashes), and the Thomas form of the point density [Eq. (9), dashed curve, arbitrarily normalized] as a function of the radius. The scale on the right margin refers to the solid curve.

MSO parametrization, with the fixed spin-orbit potential geometry, contains four fewer parameters than the STANDARD potential.

IV. INTERPRETATION OF THE MEASUREMENTS

A. Fitting procedure and results

For each of several options to describe the optical potential, the model parameters have been adjusted to fit the cross sections and analyzing power data at 122, 160, and 200 MeV. The objective criterion used for the quality of fit was the usual sum of squares of deviations, χ^2. Cross sections and analyzing powers both contributed to χ^2 weighted according to their experimental error. The total number of data points (cross section and analyzing power) at the three energies 122, 160, and 200 MeV were (53 + 52), (41 + 41), and (43 + 38), respectively. In the final fits to the data, the overall normalization of the cross section was allowed to vary, resulting in corrections of at most 9%.

Three potential options were investigated in detail. The first was the usual WS parametrization with 12 free parameters (STANDARD). In the second option the semimicroscopic spin-orbit form

factor has been used (MSO), and finally, in addition to this, a double WS shape was taken for the real central potential (DWS + MSO).

The total reaction cross section σ_R was not used to constrain the fit, since its weight relative to the rest of the data has to be chosen arbitrarily. Instead, we have compared (see Fig. 3) the σ_R, predicted by the best-fit calculations, with the available experimental data.[15–17]

B. Standard parametrization

First, we discuss the fits to the data employing the standard WS parametrization of the optical potential with 12 free parameters as defined in Sec. III A. The purpose of this is, on one hand, to generate a basis on which to judge the shape modifications discussed in the following sections and, on the other hand, to be able to compare with previous optical model analyses of ^{12}C$(p,p)^{12}$C elastic scattering data which cover a much smaller angular range. No attempt was made to obtain a smooth energy dependence of the parameters. The "best-fit" parameters at each of the three energies are listed in Table I. Calculations using this parameter set are shown in Fig. 1 and labeled STANDARD. The main difficulty with the STANDARD parametrization is its inability to account for the structure of the differential cross section at angles $\theta > 80°$ (see Fig. 1). In addition, the predicted total reaction cross section is much too large at all three energies.

Several standard optical model investigations of ^{12}C$(p,p)^{12}$C elastic scattering have previously been carried out at 122,[18] 156,[19] and 185 MeV,[18,20,21] and in the energy range 50–160 MeV.[26] It is remarkable that even at scattering angles $\theta < 80°$ there are general problems in simultaneously accounting for cross section, analyzing power, and total reaction cross
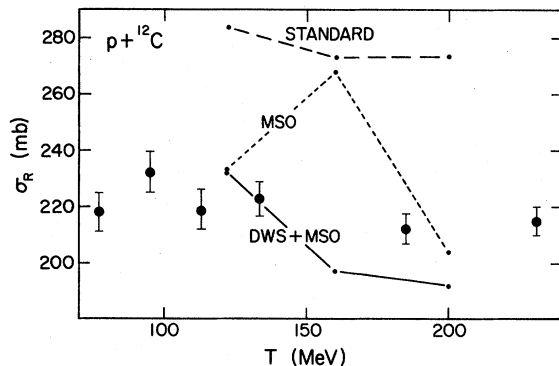
TABLE I. Best-fit parameters obtained with the STANDARD parameter option (Sec. III A), corresponding to dashed curve in Fig. 1. The geometry parameters r and a are in fm and the potential strengths in MeV.

	$T=122$ MeV	$T=160$ MeV	$T=200$ MeV
V_R	15.13	7.39	7.67
r_R	1.316	1.353	1.355
a_R	0.550	0.435	0.498
W	11.16	37.70	29.50
r_W	1.360	0.609	0.830
a_W	0.593	0.881	0.817
V_{so}	4.10	3.12	3.12
r_{Rso}	0.858	0.871	0.869
a_{Rso}	0.483	0.546	0.558
W_{so}	−1.40	−3.89	−3.11
r_{Wso}	0.810	0.815	0.872
a_{Wso}	0.442	0.567	0.522
χ_σ^2 (total)	9960	4810	3740
χ_A^2 (total)	16100	6470	3020

section. This results in a certain arbitrariness in choosing a preferred set of parameters. For example, at 185 MeV, the best-fit values quoted in the literature[18,20,21] range for the strength of the real central potential from 7.78 to 18.0 MeV, for the imaginary central potential from 6.2 to 25.7 MeV, for the real spin-orbit potential from 2.1 to 4.1 MeV, and for the imaginary spin-orbit from zero to −3.8 MeV. The fact that these parameters are so ill-determined is a clear indication of the inadequacy of the standard parametrization for describing proton scattering in this energy region.

C. Semimicroscopic spin-orbit potential

In Sec. III C we discussed the justification for replacing the standard form factor for the spin-orbit potential by a Thomas form [Eq. (9)] of the nuclear point density distribution $\rho(r)$, thus eliminating the geometry parameters for the spin-orbit potential. In this subsection we test the use of this option in an otherwise standard potential by again optimizing the fit to the data at all three energies independently. The best-fit values of the remaining eight free parameters are listed in Table II. Calculations using this parameter set are labeled MSO in Fig. 1. The improvement in χ^2 (a factor of 1.4 relative to the STANDARD set at all three energies) is substantial, considering the reduced number of free parameters. The agreement of the calculated total reaction cross section with the measured values (Fig. 3), except at 160 MeV, is also improved. This indicates that modifications of the radial shape for the spin-orbit potential are just as important as nonstandard shapes for the central potential.

FIG. 3. Total $p + ^{12}$C reaction cross section σ_R as a function of the bombarding energy. Experimental values (Refs. 15–17) are compared with values calculated using the three potential options discussed in the text with parameters as given in Tables I–III.

TABLE II. Best-fit parameters obtained with the MSO parameter option (Sec. IIIC), corresponding to dotted curve in Fig. 1. Units are the same as in Table I.

	$T=122$ MeV	$T=160$ MeV	$T=200$ MeV
V_R	15.09	9.40	7.61
r_R	1.338	1.463	1.337
a_R	0.598	0.651	0.480
W	7.20	17.01	17.88
r_W	1.328	0.706	0.981
a_W	0.758	1.095	0.702
$V_{so}{}^a$	17.64	17.32	9.77
$W_{so}{}^a$	-6.44	-6.70	-11.59
χ_σ^2 (total)	4740	4720	2960
χ_A^2 (total)	13 600	3350	2030

[a]The spin-orbit form factor is given by Eqs. (9) and (10).

One possible reason for the inferiority of the standard spin-orbit form may be the fact that the derivative of a WS shape $f(r)$ at $r=0$ is nonzero, which causes a singularity in

$$[(1/r)(d/dr)f(r)]_{r=0} .$$

For a small nucleus like ^{12}C this leads to an unphysical distortion of the normally surface-peaked spin-orbit interaction. The spin-orbit potential introduced in Eq. (9), in principle, is finite at $r=0$, although if an analytic expression is used for $\rho(r)$ this may be only approximately true. The new shape exhibits a change in sign inside of 1 fm for ^{12}C, due to the central depression in $\rho(r)$ (see Fig. 2). To illustrate these differences, the best-fit spin-orbit potentials for the STANDARD and the MSO option are compared in Fig. 4.

D. Double Woods-Saxon form for the central real potential

In this subsection we investigate the consequences of nonstandard shapes for the central potential. The particular choice of parametrization as the sum of two WS shapes (Sec. IIIB), and the fact that only the real part has to be modified, is motivated by an earlier phenomenological investigation[2] and theoretical expectations.[4] This modification is introduced in addition to the new fixed spin-orbit shape, discussed in the previous section, treating the latter as established since it significantly reduces the χ^2 *and* the number of parameters. Thus, initially, the number of free parameters in this case was 11. After a preliminary survey, however, the geometry parameters $(r_{R1}, r_{R2}, r_W, a_{R1}, a_{R2}, a_W)$ were fixed to linearly energy dependent values as indicated in Table III, and
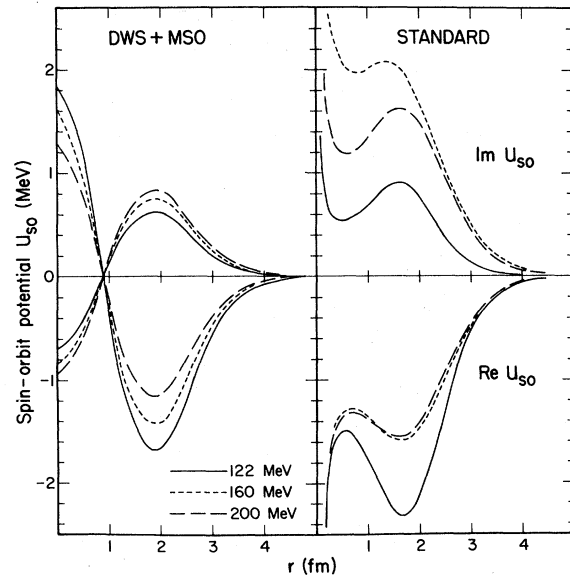

FIG. 4. Comparison of the standard form with the semimicroscopic expression for the spin-orbit potential introduced in this paper. The curves were calculated with the parameters in Tables I and II.

only the remaining *five* parameters for the potential strengths were varied. Their final best-fit values are listed in Table III. Calculations with this parameter set are shown in Fig. 2 and labeled MSO + DWS. The calculated total reaction cross sections in this case are found to be in reasonable agreement with the experiment (see Fig. 3).

The central potentials from this part of the analysis are shown as a function of the radius in panel (a) of Fig. 5. In comparing the present real central potential for 200 MeV with the one obtained earlier in our previous analysis,[2] we notice that, although the general behavior is similar, in detail the two are quite different. We have to conclude that this is due to the different parametrization of the spin-orbit potential in the two cases. Thus, it seems that the central and spin-orbit parts of the potential are not independent (a fact obvious from a Dirac equation perspective, but generally forgotten in the equivalent Schrödinger picture) and that assumptions about the *spin-orbit* parametrization strongly influence a phenomenological determination of the *central* potential (and vice versa).

The dependence of the best-fit potential strengths (as listed in Table III) on the bombarding energy T_p is monotonic. Using the same functional form as was employed in a previous global investigation of the optical model at medium energies,[6] one finds (T_p is in MeV)

$$V_1(T_p) = 439.7(1 - 0.164 \ln T_p) \; ,$$

$$V_2(T_p) = 200.5(1 - 0.138 \ln T_p) \; ,$$

$$W(T_p) = 7.6 + 2.73 \times 10^{-2}(T_p - 80)$$

$$+ 3.87 \times 10^{-6}(T_p - 80)^3 \; , \qquad (11)$$

$$V_{so}(T_p) = 70.2(1 - 0.157 \ln T_p) \; ,$$

$$W_{so}(T_p) = 11.0(1 - 0.332 \ln T_p) \; .$$

It is remarkable that the coefficients preceding the energy dependent terms are very similar to the corresponding numbers for heavier target nuclei in Ref. 6.

The dependence on bombarding energy of both real and imaginary parts of the phenomenological central potential are qualitatively in agreement with theoretical expectations. In panel (c) of Fig. 5, we show the equivalent Schrödinger potential obtained in the local density approximation[4] using an effective NN t matrix,[4] based on the Hamada-Johnston interaction and the same matter distribution $\rho(r)$, as is given by Eq. (10). As can be seen, the general features of the energy dependence of both real and imaginary parts is in good agreement with that observed for the phenomenological potential shown in panel (a). The shape of the real part, however, although showing the same general behavior, fails to reproduce details observed phenomenologically.

As we mentioned in the Introduction, another competing and unrelated theoretical approach which explains the phenomenological nonstandard potential shapes arises naturally from the use of the Dirac equation to describe elastic scattering.[22] It is noteworthy that the equivalent Schrödinger potential (i.e., the combination of Dirac potentials which appears in the second-order reduction of the Dirac equation to a Schrödinger-type form) not only exhibits nonstandard shapes near 200 MeV, but also is intrinsically energy dependent. Therefore, it is interesting to compare this intrinsic energy dependence with the one we have established phenomenologically. It can be shown[22] that the real central Schrödinger-equivalent representation of the real Dirac potentials can be written as

$$V(r) = V_s(r) + [(E + m)/m]V_0$$

$$+ (1/2m)[V_s(r)^2 - V_0(r)^2] \; , \qquad (12)$$

where $V_i(r) = V_i \cdot f_i(r)$, with $f_i(r)$ given by Eq. (6). Strengths and geometry of the scalar and vector potentials, V_s and V_0, respectively, are often treated phenomenologically in a WS parametrization. In Eq. (12), we have neglected terms containing imaginary parts and the Coulomb potential, which are much smaller than V_0 and V_s and for the present ar-

gument are considered to be lumped together with V_0 and V_s. The point we would like to make is that, with energy *independent* potentials V_0, V_s, the intrinsic energy dependence in the second term of the Schrödinger-equivalent expression to the Dirac potential, Eq. (12), is sufficient to give an excellent representation of the phenomenological energy dependence of the real central potential, as is seen by comparing panels (a) and (b) of Fig. 5. The parameters chosen for the Dirac potentials were $V_0 = 277$ MeV, $V_s = -377$ MeV, $r_0 = 0.545$ fm, $r_s = 0.504$ fm, $a_0 = 0.855$ fm, and $a_s = 0.910$ fm.

The energy dependence of the phenomenological spin-orbit potential (Table III) agrees qualitatively with the expectation from a microscopic treatment[11]: With increasing bombarding energy the absolute strength of the real part decreases monotonically while the imaginary part slowly increases. For the case of the real part this trend is also found to be reproduced by the Schrödinger-equivalent potential obtained from the Dirac equation.[22] The latter, however, predicts a *decrease* of the strength of the imaginary spin-orbit potential, which is at variance with our phenomenological finding.

We can show that the data at all three energies indeed *require* a nonstandard-shape for the central real potential. In order to demonstrate this, we have adopted the following procedure. In the framework of the DWS + MSO parametrization we have arbitrarily chosen a fixed V_{R2}. For each given value of V_{R2} we have varied the remaining nine parameters of the DWS + MSO potential (Secs. III B and III C) with a_w fixed. The resulting best-fit parameters, and the corresponding total χ^2, then depend on the choice of V_{R2}. We are interested in χ^2 as a function of, for example,

$$\alpha(V_{R2}) \equiv V_{R2}/V_{R1}(V_{R2}) \; ,$$

which measures the relative importance of the central depression, given by $V_{R2}f_{R2}(r)$, compared to the total real central potential. Thus $\alpha = 0$ would correspond to a simple WS form. Results from such a study for the 200 MeV data are shown in Fig. 6. As can be seen, $\chi^2(V_{R2})$ changes rather slowly for $V_{R2} > 4$ MeV. This is due to the fact that once V_{R2} is large enough to generate the nonstandard potential form, changes in V_{R2} can be compensated by changes in $V_{R1}(r)$ with the resulting sum potential becoming insensitive to a particular choice of V_{R2}. However, we note from Fig. 6 that χ^2 improves by a factor of 1.84 when the potential shape departs from a standard WS form ($\alpha = 0$). In the corresponding analysis of the 160 and 122 MeV data, the situation is very similar and the corresponding χ^2 improvement factors are 1.72 and 1.54, respectively.

The above technique, which imposes a change on

TABLE III. Best-fit parameters obtained with the DWS + MSO parameter option (Secs. III B and III C), corresponding to solid curve in Fig. 1. Units are the same as in Table I.

	$T=122$ MeV	$T=160$ MeV	$T=200$ MeV
	The following parameters were varied:		
V_{R1}	94.18	72.31	58.19
V_{R2}	68.17	58.84	54.50
W	9.24	11.60	17.55
V_{so}[a]	17.13	14.51	11.70
W_{so}[a]	−6.36	−7.61	−8.46
	The following parameters were fixed to linearly energy dependent values:		
r_{R1}	0.650	0.690	0.730
a_{R1}	0.780	0.740	0.700
r_{R2}	0.915	0.925	0.935
a_{R2}	0.725	0.715	0.705
r_W	1.180	1.080	0.980
a_W	0.780	0.720	0.660
χ_σ^2 (total)	6210	4190	2070
χ_A^2 (total)	7350	1420	880

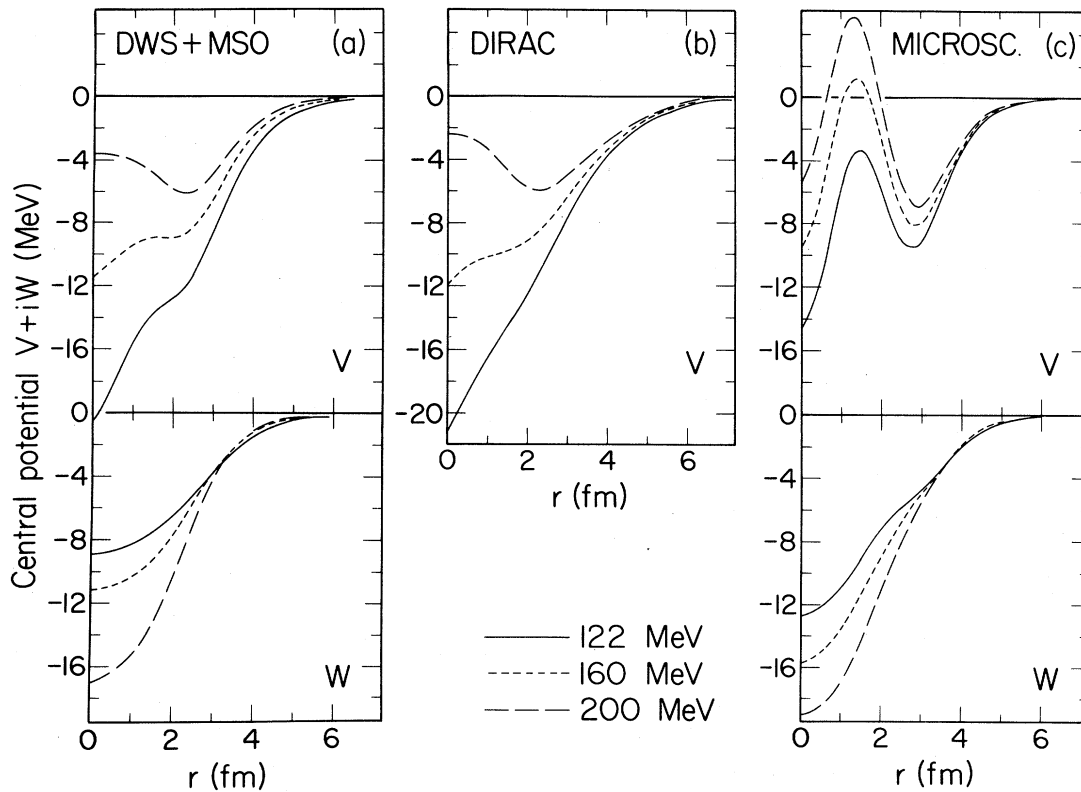[a]The spin-orbit form factor is given by Eqs. (9) and (10).

FIG. 5. The central potential $V+iW$ as a function of radius at 122, 160, and 200 MeV. The potentials in panel (a) were calculated using the parameters listed in Table III. Panel (b) represents the energy dependence predicted by a relativistic treatment, and (c) shows the corresponding potentials calculated microscopically in the local density approximation (see text).
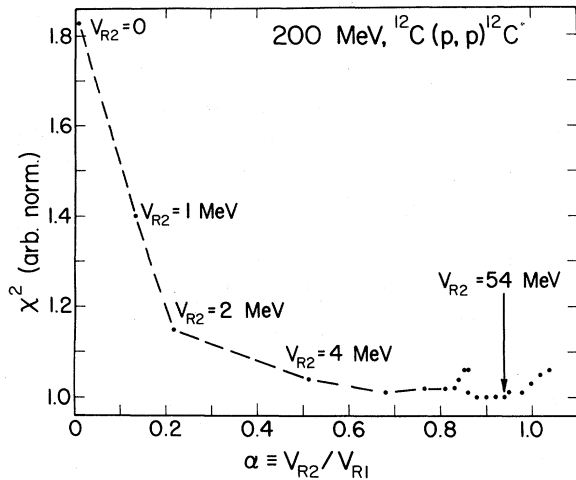
FIG. 6. Best-fit χ^2 as a function of the shape of the real central potential. The shape is determined by fixing V_{R2} in Eq. (8). The DWS + MSO potential option is used in a search on the remaining parameters. The arrow corresponds to the parameter set listed in Table III. The line is to guide the eye.
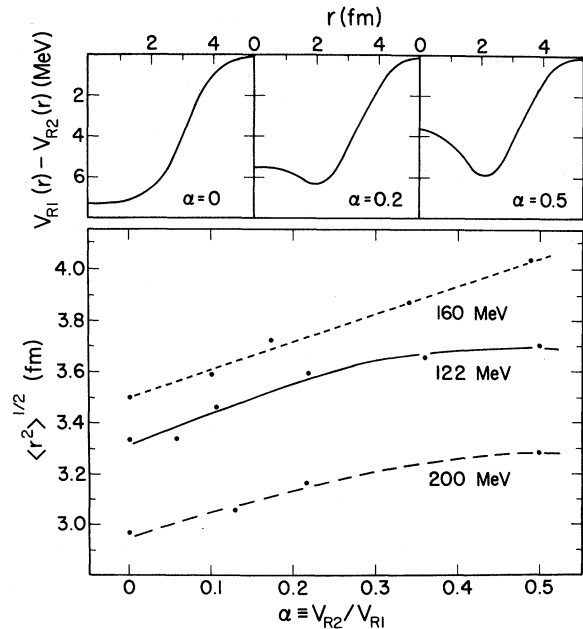

FIG. 7. Shape dependence of derived optical model parameter. In the lower part, the rms radii of the real central potential are shown for best-fit values using the DWS + MSO option constrained to a specific potential shape (shape parameter α; see text). In the upper part, radial shapes for three representative choices of α are displayed. The lines are to guide the eye.

the radial form of a potential (here the real central) by varying α (i.e., V_{R2}) is informative in yet another respect: For any choice of α we may also calculate the volume integral and the root mean square (rms) radius of the corresponding potential. For example, the resulting rms radii are shown in Fig. 7 as a function of α over the range where $V_R(r)$ develops from a simple WS form ($\alpha=0$) to a shape similar to the best-fit potential. As can be seen, variations of the rms radius of as much as 0.5 fm can occur. Similarly, the volume integral of $V_R(r)$ varies by about 25% over the same range of α. This clearly indicates that the commonly held belief that volume integrals and rms radii are parameters which are well-defined by the data and insensitive to details of the individual fit is true at best only for a given shape of the potential (e.g., a WS form).

V. CONCLUSIONS

The present investigation was prompted by the desire to study further the significance of nonstandard (e.g., non-Woods-Saxon) shapes for the real central potential found previously[2] in 200 MeV proton elastic scattering from ^{12}C. To this effect, measurements on this same target covering a similar angular range have been carried out at 160 and 122 MeV with an intent to obtain an energy dependence of these nonstandard features of the optical potential and compare phenomenological results with microscopic expectations. In view of the profusion in the literature of greatly differing best-fit standard optical potentials for ^{12}C$(p,p)^{12}$C medium energy elastic scattering, another goal was also to provide an energy dependence for the optical model description of this process. Since at 200 MeV the standard potential parametrization failed badly only when data at large momentum transfer (≥ 3 fm) were included,[2] it seems clear that any such optical model analysis must be based on angular distributions covering a large angular range.

The present work resulted in an optical potential with a simple energy dependence with only five adjusted parameters. This parametrization yields a description of the data at all three energies investigated which is much improved over the standard optical model (with 12 free parameters). The new potential differs in the radial form of the real central and the complex spin-orbit potentials and is given by the expression

$$U(r) = V_{R1}f_{R1}(r) - V_{R2}[f_{R2}(r)]^2 + iWf_W(r)$$
$$+ \lambda_\pi^{2}(V_{so} + iW_{so})g_{Mso}(r)\vec{\sigma}\cdot\vec{L} . \qquad (13)$$

The ingredients are defined in Eqs. (6), (9), and (10) and the corresponding best-fit parameters are listed

in Table III. All geometry parameters (Table III, lower portion) are linear functions of the bombarding energy, while the expressions in Eq. (12) give a good description of the energy dependence of the strength parameters (Table III, upper portion). We emphasize that this particular parametrization is not *ad hoc*, but inspired and justified by predictions of a microscopic treatment of the nucleon-nucleus optical potential.[4,11,22] The fact that such a potential leads to an improved description of the data is thus an endorsement, perhaps not of the details, but certainly of the general approach of the microscopic theory. It is also noteworthy that the phenomenological energy dependence for the potentials found in this work is qualitatively in agreement with what is expected theoretically.

Using a method to constrain the shape of the real central potential, we demonstrated that its nonstandard shape is indeed *required* by the data at all three energies investigated. By means of the same method we have also shown that the rms radii and the volume integrals of the best-fit potentials (both often believed to be quantities insensitive to details and ambiguities of the optical model) indeed depend on the assumed shape of the potential. Caution is thus required in determining the neutron rms radius $\langle r_n{}^2 \rangle^{1/2}$ from an analysis of proton scattering where the potentials are constrained to standard WS forms. Such analyses may indeed be sensitive to changes in $\langle r_n{}^2 \rangle^{1/2}$, but may not necessarily return meaningful values for $\langle r_n{}^2 \rangle^{1/2}$.

Finally, any analysis of proton *inelastic* scattering at these bombarding energies requires a justifiable choice for the distorting potential. This requirement is not serious either if such a potential is uniquely defined and physically reasonable or if there is only little sensitivity of the derived physical information

(be it details of the interaction or nuclear wave functions) on the choice of the distorting potential. It has been shown,[23,24] in an investigation of the $^{12}C(p,p')^{12}C$ reaction, that the second condition is clearly not met and hence the distorting potential in such investigations must be chosen with great care. The potential deduced in this paper is based on more experimental information than any previous prescription, is monotonic in energy, easily parametrized, and is physically reasonable (i.e., exhibits the same qualitative features as are expected from microscopic arguments), and thus may be used with some confidence to generate $p + {}^{12}C$ wave functions for bombarding energies in the range of 100–200 MeV.

Finally, we wish to point out that the present analysis, like any optical model study, is a parametrization of the data. In this context, the imaginary potential represents the sum of all effects that permanently remove flux from the elastic channel. This treatment clearly is not able to deal with dominant inelasticities, such as the excitation of the prominent 2^+ state at 4.4 MeV, where only a few terms in the partial wave sum are affected. The question whether or not coupling to the 2^+ state significantly affects an optical model analysis of the elastic scattering is currently under debate and remains to be answered. In any case, it is very unlikely that the nonstandard shape for the real central potential can be blamed on the fact that ^{12}C is a deformed nucleus, since a recent analysis of $^{16}O(p,p)^{16}O$ scattering[25] at 200 MeV also resulted in non-Woods-Saxon potential shapes.

---

[1]L. R. B. Elton, Nucl. Phys. <u>89</u>, 69 (1966).

[2]H. O. Meyer, P. Schwandt, G. L. Moake, and P. P. Singh, Phys. Rev. C <u>23</u>, 616 (1981).

[3]H. O. Meyer, J. R. Hall, W. W. Jacobs, P. Schwandt, and P. P. Singh, Phys. Rev. C <u>24</u>, 1782 (1981).

[4]F. A. Brieva and J. R. Rook, Nucl. Phys. <u>A291</u>, 299 (1977); <u>A291</u>, 317 (1977); H. V. von Geramb, F. A. Brieva, and J. R. Rook, *Lecture Notes in Physics No. 89* (Springer, Berlin, 1979), p. 104.

[5]F. A. Brieva, H. V. Geramb, and J. R. Rook, Phys. Lett. <u>79B</u>, 177 (1978).

[6]P. Schwandt, H. O. Meyer, W. W. Jacobs, A. D. Bacher, S. E. Vigdor, and M. D. Kaitchuck, Phys. Rev. C <u>26</u>, 55 (1982).

[7]J. R. Comfort, G. L. Moake, C. C. Foster, P. Schwandt,

C. D. Goodman, J. Rapaport, and W. G. Love, Phys. Rev. C <u>24</u>, 1834 (1981).

[8]P. Schwandt, Indiana University Cyclotron Facility Report No. 81-3, 1981 (unpublished).

[9]A. Nadasen, P. Schwandt, P. P. Singh, W. W. Jacobs, A. D. Bacher, P. T. Debevec, M. D. Kaitchuck, and J. T. Meek, Phys. Rev. C <u>23</u>, 1023 (1981).

[10]C. Mahaux, *Lecture Notes in Physics, No. 89* (Springer, Berlin, 1979), p. 1; B. Friedman and V. R. Pandharipande, Phys. Lett. <u>100B</u>, 205 (1981).

[11]F. A. Brieva and J. R. Rook, Nucl. Phys. <u>A297</u>, 206 (1978).

[12]J. Heisenberg, J. C. McCarthy, and I. Sick, Nucl. Phys. <u>A157</u>, 435 (1970).

[13]H. V. von Geramb, private communication.

[14]W. Bauhoff and H. V. von Geramb (unpublished).

[15]A. Johansson, U. Svanberg, and O. Sundberg, Ark. Fys. 19, 527 (1961).

[16]P. U. Renberg, D. F. Measday, M. Pepin, P. Schwaller, B. Favier, and C. Richard-Serre, Nucl. Phys. A183, 81 (1972).

[17]R. Goloskie and K. Strauch, Nucl. Phys. 29, 474 (1962).

[18]J. R. Comfort and B. C. Karp, Phys. Rev. C 21, 2162 (1980).

[19]V. Comparat, R. Frascaria, N. Marty, M. Morlet, and A. Willis, Nucl. Phys. A221, 403 (1974).

[20]A. Ingemarsson and G. Tibell, Phys. Scr. 4, 235 (1971).

[21]A. Ingemarsson, O. Jonsson, and A. Hallgren, Nucl. Phys. A319, 377 (1979).

[22]L. G. Arnold, B. C. Clark, R. L. Mercer, and P. Schwandt, Phys. Rev. C 23, 1949 (1981).

[23]J. R. Comfort, G. L. Moake, C. C. Foster, P. Schwandt, and W. G. Love, Phys. Rev. C 26, 1800 (1982).

[24]M. Hugi, W. Bauhoff, and H. O. Meyer, Indiana University Cyclotron 1982 Facility report, 1982 (unpublished).

[25]C. W. Glover, P. Schwandt, H. O. Meyer, W. W. Jacobs, J. R. Hall, M. Kaitchuck, and R. DeVito, Bull. Am. Phys. Soc. 27, 728 (1982); Indiana University Cyclotron Facility report, 1982 (unpublished).

[26]I. Abdul-Jalil and D. F. Jackson, J. Phys. G 5, 1699 (1979); D. F. Jackson and I. Abdul-Jalil, ibid. 6, 481 (1980).